PHYSICAL REVIEW E VOLUME 52, NUMBER 1 JULY 1995

Solid-fluid boundaries in particle suspension simulations via the lattice Boltzmann method

O. Behrend
Department of Physics and Astronomy, The University of Edinburgh, Mayfield Road, Edinburgh EH9 3JZ, United Kingdom
(Received 8 December 1994)

We study several possible treatments of the solid-fluid boundary in lattice Boltzmann simulations of solid-particle suspensions. Our aim is to avoid the complications of the boundary rule pioneered by Ladd [J. Fluid Mech. **271**, 285 (1994); **271**, 311 (1994)], introduced by treating the solid-fluid interactions on the links between lattice nodes rather than on the lattice nodes themselves. We show that simply treating the interactions in a similar manner on the lattice nodes is not a valid alternative due to the presence of nonrelaxing fluid distributions that do not allow steady flows to be reached. After showing the failure of the so-called "forcing method," in which the lattice velocity distributions inside the solid particle are forced to represent the local solid body velocity, we introduce a boundary treatment *at* the lattice nodes. In combination with two further simplifications in the general algorithm, this method produces results comparable to those obtained with Ladd's boundary rule, especially in the computations of bulk transport coefficients of solid-particle suspensions. When used together with a fluctuating lattice Boltzmann method, it allows for the fluctuation-dissipation theorem to be obeyed exactly at all solid-particle volume fractions.

PACS number(s): 02.70.−c, 47.15.Pn, 82.70.Dd, 82.70.Kj

I. INTRODUCTION

Suspensions of submicrometer sized particles in a liquid are found in industrial processes and products, such as paints, pharmaceuticals, ceramics, and foods, and in nature as biological fluids. There is thus considerable interest in understanding the dynamic properties of such suspensions. The theoretical description of these systems at particle volume fractions ϕ exceeding the dilute limit (say $\phi > 0.05$) is considerably complicated by the presence of indirect, or hydrodynamic, interactions between the particles. These interactions result from the velocity fields set up in the suspending liquid by the relative motion of the solid particles [1]. The treatment of these forces is complicated by the fact that they are of many-body and long-ranged nature. Numerical simulations are thus becoming an important method of studying the dynamical properties of suspensions. Most simulation algorithms such as Brownian dynamics [2], Stokesian dynamics [3], or the multipole method [4] are based on the clear time-scale separation that exists between the dynamics of the fluid and the dynamics of the solid particles. This separation implies that the development of the hydrodynamic interactions is instantaneous and that they, therefore, depend on the positions and velocities of *all* the particles. For this reason, these algorithms scale as the square or cube of the number of particles.

Very recently however, an alternative technique for such simulations has been proposed [5,6]. It is based upon the combination of Newtonian dynamics of the solid particles with a discretized Boltzmann equation (lattice Boltzmann equation, LBE) for the fluid phase. The state of the fluid is updated on a regular lattice while the solid particles (colloidal particles) move continuously in space and interact with the fluid at a set of special lattice nodes. The technique takes advantage of the fact that the hydrodynamic interactions are time dependent and develop from purely local interactions at the solid-liquid interface. Thus it is not necessary to consider the global system, but one can update one particle at a time. The method scales linearly with the number of solid particles and, therefore, allows far larger and more significant simulations than those possible with conventional methods. While the method is closely related to earlier work done by Ladd and Frenkel using lattice gas cellular automata [7,8], it does not suffer from the statistical fluctuations present in the lattice gas method. The hydrodynamic interactions between solid particles are fully accounted for with these lattice Boltzmann methods, both at zero and finite Reynolds numbers [5,6]. The crucial part of the algorithm is the mechanism of interaction between the solid particles and the fluid via the so-called "boundary rules." These boundary rules are implemented at a set of sites on the lattice, the "boundary nodes." The original method presented by Ladd [5,6] produces good results for both zero and finite Reynolds number flows. It has, however, the drawback of requiring information from two neighboring lattice nodes by placing the boundary nodes not on but in between lattice nodes. This complicates the algorithm by requiring additional information to be passed between lattice nodes.

In this paper, we will first briefly review the lattice Boltzmann algorithm for simulating fluid flows (Sec. II). We will then, after presenting the method proposed by Ladd, inspect in Sec. III several other, more simple boundary rules and evaluate their performance by applying them to simulations of particulate suspensions. We will show that placing the boundary nodes onto the lattice nodes, as was done in previous work in conjunction with the lattice gas method [7,8], leads rather unexpectedly to unsteady flows in the systems we are interested in and cannot, therefore, be used. We then present the so-

called "forcing method" in which the fluid velocity distributions inside the solid particles are forced to represent the local solid body velocity. While this method is conceptually the simplest, we will show that it cannot be used for solid-fluid suspension simulations because the hydrodynamic interactions between solid particles are not correctly reproduced. Finally, we present and analyze a set of boundary rules that, while being implemented on the lattice nodes, produces results as good as Ladd's method. We wish to emphasize that analytical developments of the effects of boundary rules are only possible for simple geometries (such as planar Couette flow). For more complex boundaries, such as in particulate suspension, such developments are not possible and the final judge of the quality of a boundary method is conceptually the numerical computation of physical quantities and the comparison of the computed values to independent calculations.

Independent of the boundary rules used, we present two modifications to the general algorithm of the lattice Boltzmann and solid-particle method that considerably simplify it. The first improvement concerns the set of boundary nodes associated with a given solid particle. In Ref. [6], this set of nodes is centered on the *lattice node* closest to the real, continuous position of the center of mass of the particle. This procedure ensures an equal number of boundary nodes for each solid particle. However, when considering moving particles, the set of boundary nodes changes abruptly when the center of mass of the particle approaches another lattice node. This can create temporary perturbations in the fluid flow. We propose a method to avoid this situation, introduced in Sec. III A 2. The second improvement concerns the so-called "shared nodes," boundary nodes for two neighboring particles. The procedure used in Ref. [6] to treat these shared nodes is rather complicated. We propose here a much simplified method, introduced in Sec. III C. We stress that these are modifications independent of the boundary method used, even though they are illustrated here in the context of specific methods.

II. THE LATTICE BOLTZMANN METHOD

The LBE method [9] has been used in recent years for a wide array of fluid-flow problems. It is based upon the discretization of space, fluid-particle velocities, and time: space is filled with a regular lattice and the fluid-particle velocity directions $\mathbf{c}_i$ are defined as the links between a given lattice node and a set of neighboring nodes. The state of the fluid at a node $\mathbf{r}$ at time t is characterized by the fluid-particle distribution functions $n_i(\mathbf{r},t)$, where the index i corresponds to velocity direction $\mathbf{c}_i$. A time step of the LBE is completed in two distinct phases: first, the distribution functions collide at the lattice nodes, where the behavior is determined by the collision operator and an equilibrium function n_i^{eq}, whose form is fixed in advance. The distribution functions are then propagated along the velocity links to the neighboring nodes, where the process is repeated. The magnitude of the velocity along link $\mathbf{c}_i$ is chosen such that the distribution function n_i propagates in a single time step to the neighboring lattice node. This leads to the following kinetic equation for the distribution functions:

$$n_i(\mathbf{r}+\mathbf{c}_i,t+1)=n_i(\mathbf{r},t)+\sum_j w_j\Delta_{ij}[n_j(\mathbf{r},t)-n_j^{\mathrm{eq}}(\mathbf{r},t)] , \tag{1}$$

where Δ_{ij} is a linearized collision operator [9,10]. The sum is over the sets of velocity directions $\mathbf{c}_i$ at node $\mathbf{r}$ and w_i is a weight associated with direction i.

The velocity directions $\mathbf{c}_i$ and their respective weights must be chosen so as to achieve isotropy of tensors of the fourth rank formed from sums over the sets of directions [9,11,12]. They must satisfy the following relations:

$$\sum_i w_i=b, \quad \sum_i w_i c_{i\alpha}=0 ,$$

$$\sum_i w_i c_{i\alpha}c_{i\beta}=\frac{bc^2}{D}\delta_{\alpha\beta}, \quad \sum_i w_i c_{i\alpha}c_{i\beta}c_{i\gamma}=0 ,$$

$$\sum_i w_i c_{i\alpha}c_{i\beta}c_{i\gamma}c_{i\delta}=\frac{bc^4}{D(D+2)} \times[\delta_{\alpha\beta}\delta_{\gamma\delta}+\delta_{\alpha\gamma}\delta_{\beta\delta}+\delta_{\alpha\delta}\delta_{\beta\gamma}] . \tag{2}$$

Greek subscripts denote spatial indices, $\delta_{\alpha\beta}$ is the Kronecker δ function and b, D, and c^2 are parameters that, while their notation derives from the lattice gas formalism, must be regarded as defined by the above equations and depend on the lattice on which the LBE is based [12].

From the distribution functions n_i, hydrodynamic fields can be constructed in a similar way as they are in kinetic theory from the one-particle velocity distribution function [13]. The mass density ρ, the momentum density $\mathbf{j}=\rho\mathbf{u}$, and the momentum flux or fluid stress $\mathbf{\Pi}$ are

$$\rho=\sum_i w_i n_i, \quad \mathbf{j}=\sum_i w_i n_i \mathbf{c}_i, \quad \mathbf{\Pi}=\sum_i w_i n_i \mathbf{c}_i\mathbf{c}_i . \tag{3}$$

The equilibrium function is chosen so that after a multiscale expansion and in the low-Mach-number approximation, the incompressible Navier-Stokes equations are obtained [9,11]. It can be expressed as a series expansion in powers of the flow velocity $\mathbf{u}$ [6,9],

$$n_i^{\mathrm{eq}}=\rho(A_i+B_i\mathbf{u}\cdot\mathbf{c}_i+C_i\overline{\mathbf{uu}}:\overline{\mathbf{c}_i\mathbf{c}_i}+D_i u^2) , \tag{4}$$

with

$$A_i=\frac{1}{b}, \quad B_i=\frac{D}{bc^2}, \quad C_i=\frac{D(D+2)}{2bc^4} ,$$

$$D_i=\frac{D(D+2)}{2bc^4}\frac{D}{D-d}\left[\frac{c_i^2}{d}-\frac{c^2}{D}\right] , \tag{5}$$

where d is the spatial dimension, $\overline{\mathbf{uu}}$ is the traceless part of $\mathbf{uu}$, and the double dot product is defined as $\mathbf{A}:\mathbf{B}=\sum_{\alpha,\beta}A_{\alpha\beta}B_{\beta\alpha}$.

By choosing n_i^{eq} to linear order in the velocity field

$$n_i^{\mathrm{eq}}=\rho(A_i+B_i\mathbf{u}\cdot\mathbf{c}_i) , \tag{6}$$

the Stokes (or creeping-flow) equations are recovered [1]

in the long-time limit, corresponding to a flow regime at zero Reynolds number.

A simplification of the full LBE model is the lattice BGK model (so-called in analogy with the Bhatnagar-Gross-Krook approximation to the Boltzmann equation [14]) [12,15,16], in which the collision operator Δ_{ij} is such that the distribution functions are simply relaxed at each time step towards the local equilibrium n_i^{eq} with relaxation time τ:

$$n_i(\mathbf{r}+\mathbf{c}_i,t+1)=n_i(\mathbf{r},t)-\frac{n_i(\mathbf{r},t)-n_i^{eq}(\mathbf{r},t)}{\tau} . \quad (7)$$

The parameter τ controls the relaxation of the viscous stress in the fluid [12] and is linked to the kinematic viscosity ν via the relation [16]

$$\nu=\frac{c^2(2\tau-1)}{2(D+2)} . \quad (8)$$

A linear stability analysis indicates that τ must be greater than $\frac{1}{2}$, which also ensures that the kinematic viscosity is positive.

An additional simplification is obtained when $\tau=1$, in which case the distributions relax immediately to their equilibrium value and Eq. (7) becomes

$$n_i(\mathbf{r}+\mathbf{c}_i,t+1)=n_i^{eq}(\mathbf{r},t) . \quad (9)$$

The disadvantage of the choice $\tau=1$ is that it gives a relatively high viscosity [Eq. (8)]. However, especially for flows at zero Reynolds number (creeping-flow regime), the viscosity is not a critical parameter and $\tau=1$ therefore represents a useful simplification.

The simulations in this paper were done using a lattice-BGK model on a 14-link lattice (model D3Q14 of Ref. [12]), which requires somewhat less storage than the more usual 18-link lattice [6,11]. In the 14-link lattice, the velocity directions $\mathbf{c}_i$ link each lattice node of a simple cubic lattice to its nearest (1 0 0) and next-next-nearest (1 1 1) neighbors. The parameters for this model are $b=56$, $c^2=3$, and $D=7$ and the weights are $w_i=8$ for the nearest and $w_i=1$ for the next-next-nearest-neighbor links.

In what follows, we will use t_+ to indicate the time immediately after the LBE collision, preceding the propagation of the distribution functions. Therefore [see Eq. (7)],

$$n_i(\mathbf{r},t_+)=n_i(\mathbf{r},t)-[n_i(\mathbf{r},t)-n_i^{eq}(\mathbf{r},t)]/\tau . \quad (10)$$

III. THE SOLID-FLUID BOUNDARY

The general idea of the treatment of boundaries between the solid particles (referred to also as "particles" in the following) and the fluid is the same for all the methods presented in this paper. A solid particle is mapped onto the lattice and defines a set of boundary nodes whose positions are $\mathbf{r}_b$. At each update of the lattice, a special rule at the boundary nodes is implemented on the distribution functions n_i. This boundary rule exchanges momentum between the fluid and the particle (note however that the combined momentum of the fluid and the solid phase is conserved) and enforces a stick boundary condition on the fluid, i.e., the fluid velocity at the boundary nodes is matched to the local solid-body velocity $\mathbf{u}_b$. $\mathbf{u}_b$ is determined by the solid-particle velocity $\mathbf{U}$, its angular velocity $\mathbf{\Omega}$, and the position of its center of mass $\mathbf{R}$,

$$\mathbf{u}_b=\mathbf{U}+\mathbf{\Omega}\times(\mathbf{r}_b-\mathbf{R}) . \quad (11)$$

The momentum density exchange causes a local force density to be exerted on the particle at node $\mathbf{r}_b$, $\mathbf{f}(\mathbf{r}_b)$, and the total force and torque on the particle are obtained by summing $\mathbf{f}(\mathbf{r}_b)$ and $(\mathbf{r}_b-\mathbf{R})\times\mathbf{f}(\mathbf{r}_b)$ over all the boundary nodes associated with the particle. These forces and torques are used to update the position and velocities of the particle according to the laws of Newtonian mechanics, using a preassigned mass and moment of inertia.

A. The generalized bounce-back rules

We consider in this section the general boundary method developed by Ladd [6] and Ladd and Frenkel [7]. In Sec. III A 1, we quickly review its most recent implementation, the method used in Ref. [6] with boundary nodes placed in between lattices nodes. In Sec. III A 2, we show that placing the boundary nodes on the lattice nodes is not a possible alternative.

To enforce a stick boundary condition on a stationary boundary, the so-called "bounce-back rule" has been used extensively in lattice gas and lattice Boltzmann methods [17,18]. In this method, the stick condition is enforced by reflecting, at a boundary node, the incoming populations on link $\mathbf{c}_i$ back into the direction $\mathbf{c}_{-i}\equiv-\mathbf{c}_i$. For moving boundaries, a generalization of the bounce-back rule has been developed by Ladd and Frenkel [7,8]. The idea is to modify the incoming distributions by exchanging momentum between the two sides of the boundary so as to change the local fluid velocity and implement a no-slip boundary condition at the required local velocity $\mathbf{u}_b$; this will be illustrated in the following paragraphs. An important feature of the generalized boundary rule is that the added force density does not modify the local velocity gradients (or shear stresses) so that the velocity gradients at the boundary match those in the interior of the fluid. This prevents the formation of an additional boundary layer by the momentum density exchange [8]. The interior and exterior of the particle are treated in a similar fashion, resulting in fluid on both sides of the boundary nodes. It can be shown [6] that in the creeping-flow regime, the interior fluid only contributes an additional mass and moment of inertia to the particle.

1. Bounce back on the links (BBL)

In the most recent implementation of the generalized bounce-back rule, the boundary nodes are placed in between lattice nodes. The solid particles are mapped onto the lattice in the following manner. A spherical surface of radius a (in what follows we will consider only spherical particles; however, any shape particle could be used), is placed onto the lattice, centered at the position $\mathbf{R}$ of the center of mass of the particle. It cuts a set of links $\mathbf{c}_i$

and the boundary nodes are placed halfway on these links, as illustrated in Fig. 1(a) (note that in Figs. 1–4, we have chosen for simplicity a simple square lattice as the underlying lattice; this is not representative of the lattice used in the simulations). A more precise representation of the particle surface will be obtained if a larger input radius a (measured in terms of lattice spacings) is chosen. We note that the solid particles do not have to be centered on a lattice node, so that $\mathbf{R}$ is a continuous variable. Thus, the number of boundary nodes for a given surface can vary from location to location. We will come back to this point in Sec. III A 2.

A time step of the algorithm proceeds as follows: the LBE collisions are done at all lattice nodes and the populations are propagated along their respective links. If a link is occupied by a boundary node $\mathbf{r}_b=\mathbf{r}+\frac{1}{2}\mathbf{c}_i$ [Fig. 1(b)], there are two incoming populations $n_i(\mathbf{r},t_+)$ and $n_{-i}(\mathbf{r}+\mathbf{c}_i,t_+)$. The velocity associated with the boundary node $\mathbf{u}_b$ is defined by Eq. (11). For a stationary boundary, $\mathbf{u}_b=0$, the incoming populations are reflected,

$$\begin{aligned} n_i(\mathbf{r}+\mathbf{c}_i,t+1)&=n_{-i}(\mathbf{r}+\mathbf{c}_i,t_+)\ , \\ n_{-i}(\mathbf{r},t+1)&=n_i(\mathbf{r},t_+)\ . \end{aligned} \tag{12}$$

When $\mathbf{u}_b\neq 0$, momentum density is transferred across the boundary surface, in the direction of movement of the colloidal particle,

$$\begin{aligned} n_i(\mathbf{r}+\mathbf{c}_i,t+1)&=n_{-i}(\mathbf{r}+\mathbf{c}_i,t_+)+2B_i\rho\mathbf{u}_b\cdot\mathbf{c}_i\ , \\ n_{-i}(\mathbf{r},t+1)&=n_i(\mathbf{r},t_+)-2B_i\rho\mathbf{u}_b\cdot\mathbf{c}_i\ , \end{aligned} \tag{13}$$

where B_i is the same constant as in Eq. (4).

By rearranging the populations only among opposite pairs of velocities, the local mass density and the stress tensor (which are both even moments of the velocities) are not modified. The exact form and amount of momentum density transferred ensures that any distribution function with velocity $\mathbf{u}=\mathbf{u}_b$ is unchanged by the collision rule [6]. It can also be shown that the hydrodynamic stick conditions apply exactly at $\mathbf{r}_b$ [6].

As shown by Ladd [6], this method works well in simulating solid-fluid suspensions both in the creeping-flow regime and at higher Reynolds numbers. Transport coefficients of particle suspensions are obtained with good accuracy at all solid concentrations for particles with radii of the order of 4–8 lattice spacings. However, as apparent from the above description of the method, its implementation requires that information between two neighboring lattice sites (the sites enclosing the boundary node) is exchanged, therefore, complicating the simple update of the LBE method.

2. *Bounce back at the nodes (BBN)*

The obvious way around the complication noted above is to place the boundary nodes *on* the lattice nodes, as done in the early simulations of Ladd and Frenkel [8]. The lattice nodes that are the closest to the shell of radius a placed on the lattice are marked as boundary nodes. This is illustrated in Fig. 2. An immediate drawback of this method is that because there are less boundary nodes for a given size particle, the resolution is reduced in this method.

A time step of the algorithm proceeds as follows: the LBE collisions are done at all lattice nodes *except* at the boundary nodes. At the boundary nodes, for a stationary boundary $\mathbf{u}_b=0$, the populations $n_i(\mathbf{r}_b,t)$ and $n_{-i}(\mathbf{r}_b,t)$ are exchanged for all velocity directions. This is the method studied by Cornubert, d'Humières, and Levermore [17] and they showed that the stick boundary condition then applies at halfway between the boundary node

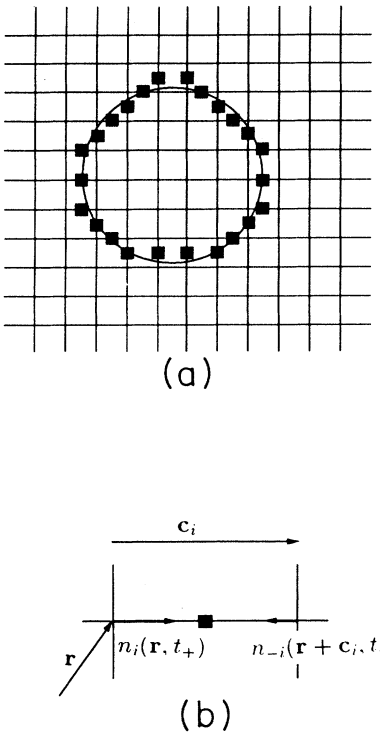

FIG. 1. (a) Mapping of a circular particle onto a square lattice for the BBL method. The boundary nodes are marked by the black squares, (b) definition of nodes and distributions for the BBL method.

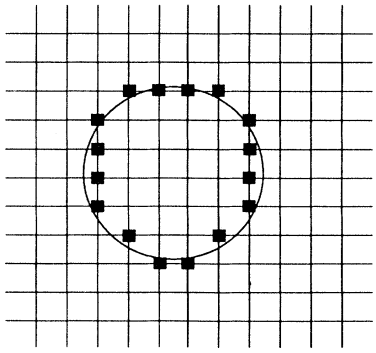

FIG. 2. Mapping of a circular particle onto a square lattice for the BBN method. The boundary nodes are marked by the black squares.

and the first fluid node. By not implementing LBE collisions at the boundary nodes, the stresses on either side of the boundary are left unchanged and thus the velocity gradients near the boundary are continuous.

For a moving boundary, $\mathbf{u}_b \neq 0$, momentum density is exchanged as for the BBL method,

$$\begin{aligned} n_i(\mathbf{r}_b+\mathbf{c}_i,t+1)&=n_{-i}(\mathbf{r}_b,t)+2B_i\rho\mathbf{u}_b\cdot\mathbf{c}_i \ , \\ n_{-i}(\mathbf{r}_b-\mathbf{c}_i,t+1)&=n_i(\mathbf{r}_b,t)-2B_i\rho\mathbf{u}_b\cdot\mathbf{c}_i \ . \end{aligned} \tag{14}$$

Again, mass and stress are not influenced by this exchange of momentum density. It can be shown that the stick boundary conditions apply, as for stationary boundaries, at $\mathbf{r}_b+\frac{1}{2}\mathbf{c}_i$ into the fluid. Thus, no *additional* boundary layer is set up.

This method has been used and studied extensively for stationary boundaries and some calculations on moving boundaries have been successful in conjunction with the lattice gas method [8]. However, we have found during this study that this method generates unphysical behavior when used for the simulation of particulate suspensions or, more generally, for closely spaced boundaries of similar velocity. Indeed, we noticed that no steady fluid flows could be reached at a high volume fraction and thus no steady forces could be reached. We believe that this is due to the following mechanism. At high particle concentrations, it is very likely that two neighboring lattice nodes are boundary nodes for two different particles. Taking $\mathbf{r}_1$ and $\mathbf{r}_2=\mathbf{r}_1+\mathbf{c}_i$ as the positions of the two nodes and as $\mathbf{u}_{b_1}$ and $\mathbf{u}_{b_2}$ the local solid-body velocities at $\mathbf{r}_1$ and $\mathbf{r}_2$, respectively, we can show that the two distribution functions $n_{-i}(\mathbf{r}_1)$ and $n_i(\mathbf{r}_2)$ are isolated from the rest of the fluid. Starting at time t with $n_{-i}(\mathbf{r}_1,t)$ and $n_i(\mathbf{r}_2,t)$, after one time step we have

$$\begin{aligned} n_{-i}(\mathbf{r}_1,t+1)&=n_i(\mathbf{r}_2,t)-2B_i\rho\mathbf{u}_{b_2}\cdot\mathbf{c}_i \ , \\ n_i(\mathbf{r}_2,t+1)&=n_{-i}(\mathbf{r}_1,t)+2B_i\rho\mathbf{u}_{b_1}\cdot\mathbf{c}_i \ , \end{aligned} \tag{15}$$

and after a further time step, supposing $\mathbf{u}_{b_1}$ and $\mathbf{u}_{b_2}$ change negligibly

$$\begin{aligned} n_{-i}(\mathbf{r}_1,t+2)&=n_i(\mathbf{r}_2,t+1)-2B_i\rho\mathbf{u}_{b_2}\cdot\mathbf{c}_i \\ &=n_{-i}(\mathbf{r}_1,t)+2B_i\rho\mathbf{u}_{b_1}\cdot\mathbf{c}_i-2B_i\rho\mathbf{u}_{b_2}\cdot\mathbf{c}_i \ , \\ n_i(\mathbf{r}_2,t+2)&=n_{-i}(\mathbf{r}_1,t+1)+2B_i\rho\mathbf{u}_{b_1}\cdot\mathbf{c}_i \\ &=n_i(\mathbf{r}_2,t)-2B_i\rho\mathbf{u}_{b_2}\cdot\mathbf{c}_i+2B_i\rho\mathbf{u}_{b_1}\cdot\mathbf{c}_i \ . \end{aligned} \tag{16}$$

Since the relative mobility of a pair of almost touching spheres is small, $\mathbf{u}_{b_1}$ and $\mathbf{u}_{b_2}$ are very similar so that

$$\begin{aligned} n_{-i}(\mathbf{r}_1,t+2)&\simeq n_{-i}(\mathbf{r}_1,t) \ , \\ n_i(\mathbf{r}_2,t+2)&\simeq n_i(\mathbf{r}_2,t) \ . \end{aligned} \tag{17}$$

It is thus apparent that these two populations will bounce back and forth between the two boundary nodes without being relaxed by LBE collisions and, therefore, without relaxing to the general fluid motion. At high concentrations, the number of enclosed links can be significant and will hinder the establishment of a steady flow in the system. We tested the hypothesis presented here by generating configurations of colloidal particles such that no enclosed links were present and we were then able to reach steady flows. However, such configurations are not thermodynamic equilibrium distributions and they will, therefore, not yield correct transport coefficients, even at low volume concentrations. The calculations of hydrodynamic interactions between pairs of spheres of Ref. [8] were possible because the spheres were forced to have equal and *opposite* velocities. This situation will usually not occur in many-particle suspensions.

This result does not seem to have been appreciated so far: the choice of the BBL method in previous work was mainly motivated by the better resolution of the particle surface that this method provides [6].

Note that the situation where two adjacent lattice nodes are boundary nodes for the *same* solid particle can also arise. Following the same reasoning as above, it is clear that trapped populations can also exist in that case. However these populations, contained *within* the solid particle, will not influence the flow outside the particle and their effect is, therefore, not felt in the same manner.

Before presenting alternative boundary methods, we wish to address the question of the set of boundary nodes associated with a solid particle and the definition of the so-called hydrodynamic radius of a particle. This will lead to the introduction of the first of the two modifications we propose to simplify and improve the general LBE and solid-particle algorithm. While each of the presented boundary methods uses a different mapping of the solid particles onto the lattice, this discussion remains valid for all those methods.

Due to the discrete nature of the particle surface on the lattice, it is impossible to determine an exact value for the radius *a priori*. It is thus necessary to compute a hydrodynamic radius, obtained by fitting the computed low-volume-fraction translational drag of a periodic array of spheres $\xi^T=F_D/U_V$ (where F_D is the drag force and U_V the volumetric flow in the unit cell) to the asymptotic expression [19]

$$\frac{6\pi\eta}{\xi^T}=\frac{1}{a}-\frac{2.827}{L}+\frac{4.19}{L^3}a^2-\frac{27.4}{L^6}a^5 \ . \tag{18}$$

The periodic array is obtained by applying periodic boundary conditions to a central cell containing a single sphere, L being the edge size of this central cell. η is the viscosity of the fluid. Closely related to the computation of the hydrodynamic radius is the definition of the actual set of boundary nodes that represent each solid particle. Whereas in Ref. [6] each particle has an *identical* set of boundary nodes (determined by mapping onto the lattice the sphere of radius a centered *on the lattice node* closest to the actual position $\mathbf{R}$ of the particle), here we prefer to determine the boundary nodes by using the sphere of radius a centered *on the actual position* $\mathbf{R}$. This has the clear advantage that the set of boundary nodes moves

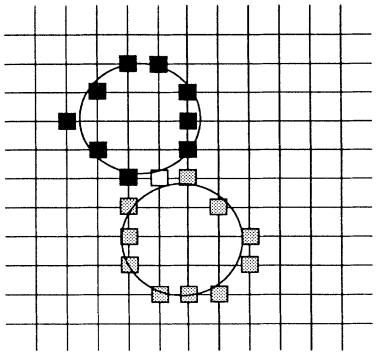

FIG. 3. Two different mappings for two particles of the same input radius for the BBN method. The white square (□) marks a shared node between the two particles.

more continuously with the position **R** of the particle and it thus avoids large perturbations of the fluid flow as the set of boundary nodes is changed. However, the set of boundary nodes will vary from particle to particle and with time as the particle positions change. This is illustrated in Fig. 3 with the BBN mapping. The set of boundary nodes determines the interactions of the particle with the surrounding fluid and thus influences the hydrodynamic radius. We solve this problem by determining an *average* hydrodynamic radius a_H from a random sample of particle locations (typically of the order of 100) and averaging the corresponding hydrodynamic radii. The statistical errors in the average radius are then of the order of 1 part in 1000.

B. Forcing method (FM)

We investigate in this section a method proposed by Chen *et al.* [20] that differs considerably from the generalized bounce-back scheme but that is perhaps intuitively more attractive.

In the FM, the particle is mapped onto the lattice in a very simple way: all the lattice nodes within the shell of radius a are "boundary nodes" (Fig. 4). This appellation

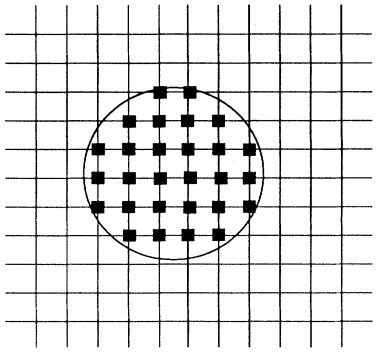

FIG. 4. Mapping of a circular particle onto a square lattice for the FM method. The boundary nodes are marked by the black squares.

is not quite correct here since nodes in the interior of the particle are not on its boundary, but we will continue to use this term to denote those lattice nodes where a special "boundary rule" is implemented. The boundary rule at the boundary nodes takes effect at the same time as the LBE collision at the fluid nodes: instead of updating the distribution functions according to Eq. (7), they are forced to the equilibrium distribution corresponding to a local velocity $\mathbf{u}_b(\mathbf{r}_b)$ [Eq. (11)]

$$n_i(\mathbf{r}_b+\mathbf{c}_i,t+1)=\rho(\mathbf{r}_b,t)[A_i+B_i\mathbf{c}_i\cdot\mathbf{u}_b(\mathbf{r}_b,t)] \tag{19}$$

for a creeping-flow simulation. The fluid distributions inside the particle are thus forced to represent the solid-body motion, $\mathbf{u}(\mathbf{r}_b)=\mathbf{u}_b(\mathbf{r}_b)$.

It is clear from the above description that the stresses are not conserved by the boundary rule; they are forced to their equilibrium value. Thus, a boundary layer is created in which the velocity gradients inside the fluid match their equilibrium value at the particle boundary. It can be shown [21] that for planar Couette flow, the stick boundary condition holds at $\mathbf{r}_b+x_0\mathbf{c}_i$ into the fluid, where $x_0=1-\tau$ and τ is the relaxation parameter of the viscous stresses [Eq. (7)]. Thus, when $\tau=1$, and the stresses are immediately relaxed to their equilibrium value in the fluid, no boundary layer is present. This analysis is valid for simple shear flow in two dimension but for more complicated boundaries in three dimensions, as present in colloidal suspensions, no such analytical treatment is possible. Therefore, to judge the value of this boundary method, we compare computations of different transport coefficients using the LBE method coupled with these boundary rules to independent numerical calculations [4].

We have computed the following quantities for suspensions of 16 spheres: the permeability of a fixed configuration (K), the short-time collective mobility (μ), and the short-time self-diffusion (D_s). The permeability relates the volume-averaged velocity of the fluid through a configuration of spheres to the applied pressure gradient. The collective mobility describes the motion of the configuration of spheres under the influence of an exterior force and is, therefore, related to the sedimentation velocity of the configuration. The self-diffusion describes the motion of a single sphere within the configuration under the influence of an external force. It should be noted that we are considering instantaneous equilibrium particle configurations and thus measurements on a time scale sufficiently short that the particles do not move over distances comparable to their radius. The diffusion coefficient measured is, therefore, the short-time diffusion. These simulations are based on dissipative methods and the exact methodology is described in detail in Ref. [6] and will not be further discussed here.

The results we report here were obtained with $\tau=1$. They are averaged over 96 equilibrium distributions of spheres, generated with a standard hard-sphere Monte Carlo program, and are shown in Fig. 5 for a number of different sized spheres (the radii a_H being expressed in terms of lattice units) to illustrate the convergence of the method with the radius of the particles.

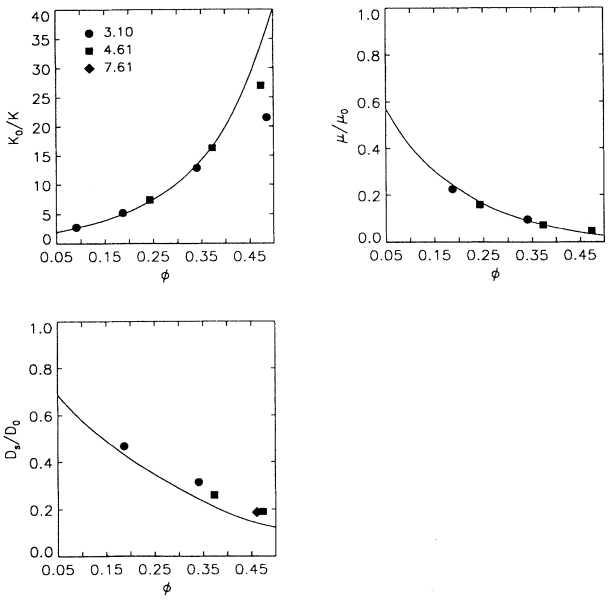

FIG. 5. Transport coefficients for 16 spheres as a function of volume fraction obtained with the FM boundary method. The solid curves are independent numerical calculations [4] and can be considered exact. The radii are in terms of lattice spacings. K_0/K is the normalized inverse permeability, μ/μ_0 the normalized collective mobility and D_s/D_0 the normalized short-time self-diffusion. The statistical errors are smaller than the plotting symbols.

The results for the inverse permeability K^{-1} are normalized by its low density limit $K_0^{-1}=\frac{9}{2}\phi/a_H^2$, where ϕ is the solid-particle volume fraction. They compare rather well with the independent computations, except at high volume fraction, where very large particles would be necessary for accurate results. The collective mobility μ, normalized by the isolated-sphere result $\mu_0=(6\pi\eta a_H)^{-1}$, is obtained quite accurately with relatively small spheres. However, the FM method clearly fails in the computation of the short-time self-diffusion D_s (normalized here by the isolated-sphere result $D_0=k_BT\mu_0$, where k_B is the Boltzmann constant and T the temperature). Throughout the concentration range, results are too large and the results do not seem to improve by increasing the particle size. We were able to obtain better results by lowering the kinematic viscosity ν of the fluid [see Eqs. (7) and (8)]. However, it was impossible to get consistently good results over the whole range of volume fraction: the viscosity can be tuned so as to produce an acceptable result at a given volume fraction, but this same viscosity would then produce poor results at other volume fractions. Moreover, by lowering the viscosity, the transient hydrodynamic time $\tau_H=a_H^2/\nu$ is increased and thus the length of the simulation increases proportional to ν^{-1}. The self-diffusion coefficient D_s depends strongly on the hydrodynamic interactions between particles [22] and especially on the lubrication forces when the particles are near contact. Computations of two-body hydrodynamic forces with the FM method have shown that these forces are not obtained correctly at particle separations of about 1–2 lattice spacings—our calculations show that the forces are underestimated by 20–25 % for the particle radii used in the computations presented here. This might be the reason for not obtaining the correct self-diffusion over the whole range of volume fractions and the permeability at high volume fraction. It is, however, not entirely clear yet why the FM method fails to reproduce the two-body hydrodynamic interactions. A possible cure to this problem might be to include the lubrication forces explicitly in the simulation, as is done for simulations using Stokesian dynamics [3]. However, since our results are equally poor throughout the particle concentration range, it is not quite sure if this modification would improve the results significantly.

C. Relaxed bounce back at the nodes (RBBN)

We present in this section a boundary method that, while treating the fluid-solid interactions on the lattice nodes, produces good results in the calculation of transport coefficients. To our knowledge, it has not been applied before, but is similar to a method proposed by Ziegler [18] for stationary plane walls. We will also present the second proposed improvement to the general LBE and solid-particle algorithm concerning the shared boundary nodes.

The motivation for the RBBN method is to improve the results of the BBN method by avoiding the problem of the "trapped" distributions. The main observation is that for the BBL method, even though two adjacent boundary nodes might be boundary nodes for different particles, leading to distributions trapped between two boundary nodes, these populations are relaxed at each time step by the LBE collisions. The method presented here is a combination of the BBL and BBN methods. The boundary nodes are located *at* the lattice nodes, but the LBE collisions are done at *every* lattice node, including the boundary nodes. Using the same definition of boundary nodes as for the BBN method (Fig. 2), the update at the boundary nodes is now

$$\begin{aligned} n_i(\mathbf{r}_b+\mathbf{c}_i,t+1)&=n_{-i}(\mathbf{r}_b,t_+)+2B_i\rho\mathbf{u}_b\cdot\mathbf{c}_i \\ n_{-i}(\mathbf{r}_c-\mathbf{c}_i,t+1)&=n_i(\mathbf{r}_b,t_+)-2B_i\rho\mathbf{u}_b\cdot\mathbf{c}_i\ . \end{aligned} \tag{20}$$

It can readily be seen that even though the exchange of momentum density itself leaves the local stresses unchanged, the incoming information about the velocity gradients contained in $n_i(\mathbf{r},t)$ is modified by the LBE collisions leading to $n_i(\mathbf{r},t_+)$. The velocity gradients at the boundary will, therefore, not match the velocity gradients in the interior of the fluid. As will be seen in what follows, this leads to the creation of a thin boundary layer and somewhat modified fluid velocity distributions inside the wall.

As an idealized model of what is happening at the boundary of a solid particle, we study a plane boundary wall moving at velocity $u_0\mathbf{e}_y$ between a uniform flow (representing the flow inside the particle) and a simple shear flow (representing the flow outside). We assume that the flows are time independent and invariant under translation in the y and z directions and work with a

two-dimensional projection into the xy plane of the 14-link model [12], as presented in Fig. 6. We recall that the parameters for this model are $b=56$, $D=7$, and $c^2=3$ and the weights are $w_i=8$ for the (1 0) directions and $w_i=1$ for the (1 1) directions. Working at a low Reynolds number, we use the linear approximation to the equilibrium distribution function [Eq. (6)]. The problem is to find the distribution functions that are stationary under the boundary rules at the wall ($x=0$) and that represent a uniform flow for $x<0$ and a shear flow with uniform velocity gradient γ for $x>0$. (A similar problem has been solved for the BBL method in Ref. [6].) We will show in the following development that an exact linear shear flow with velocity gradient γ is generated in the exterior fluid and that the interior fluid moves at uniform velocity $u_0-\gamma/12$. A boundary layer of width $\frac{1}{12}$ is set up.

The velocity distribution for the uniform flow for $x<0$ is the equilibrium distribution,

$$\begin{aligned} &n_0(x)=2,\quad n_1(x)=1,\quad n_{-1}(x)=1\ ,\\ &n_2(x)=1+\tfrac{7}{3}u_u,\quad n_{-2}(x)=1-\tfrac{7}{3}u_u\ ,\\ &n_3(x)=2(1+\tfrac{7}{3}u_u),\quad n_{-3}(x)=2(1-\tfrac{7}{3}u_u)\ ,\\ &n_4(x)=2(1-\tfrac{7}{3}u_u),\quad n_{-4}(x)=2(1+\tfrac{7}{3}u_u)\ . \end{aligned} \tag{21}$$

Here $u_u\mathbf{e}_y$ is the flow velocity and the mass density has been set equal to $\rho=b=56$ for convenience. The distributions of the (1 1) directions ($i=\pm3,\pm4$) have been multiplied by two to account for the number of projections from the three-dimensional lattice giving the same velocity direction in two dimensions [for example, (1 1 1) and (1 1 $\bar{1}$) both project onto (1 1)]. Another feature of this two-dimensional projection is the appearance of a rest particle ($i=0$) which results from the projections of the (0 0 1) and (0 0 $\bar{1}$) links; it's distribution function is thus also multiplied by two. These distributions are the equilibrium distributions and are unchanged by the LBE collisions [Eq. (7)]. As they are x independent, they are not modified by the propagation step. Thus, for $x<1$, these distributions are stationary.

The expected distribution in the shear flow with uniform velocity gradient for $x>0$ is the equilibrium distribution with $\mathbf{u}=[u_0+\gamma(x-x_0)]\mathbf{e}_y$ plus the nonequilibrium distribution [6,11]

$$n_i^{\rm neq}=-\tfrac{7}{3}\tau c_{i_x}c_{i_y}\ . \tag{22}$$

The offset x_0 allows for the inclusion of a boundary layer. Thus, for $x>0$,

$$\begin{aligned} &n_0(x)=2,\quad n_1(x)=1,\quad n_{-1}(x)=1\ ,\\ &n_2(x)=1+\tfrac{7}{3}[u_0+\gamma(x-x_0)]\ ,\\ &n_{-2}(x)=1-\tfrac{7}{3}[u_0+\gamma(x-x_0)]\ ,\\ &n_3(x)=2\{1+\tfrac{7}{3}[u_0+\gamma(x-x_0)]-\tfrac{7}{3}\tau\gamma\}\ ,\\ &n_{-3}(x)=2\{1-\tfrac{7}{3}[u_0+\gamma(x-x_0)]-\tfrac{7}{3}\tau\gamma\}\ .\\ &n_4(x)=2\{1-\tfrac{7}{3}[u_0+\gamma(x-x_0)]+\tfrac{7}{3}\tau\gamma\}\ ,\\ &n_{-4}(x)=2\{1+\tfrac{7}{3}[u_0+\gamma(x-x_0)]+\tfrac{7}{3}\tau\gamma\}\ . \end{aligned} \tag{23}$$

The post-collision distributions are calculated from Eqs. (3), (6), and (7) and propagated to the neighboring nodes. For $x>1$, the new distributions, noted $n_i'(x)$ are then,

$$\begin{aligned} &n_0'(x)=2,\quad n_1'(x)=1,\quad n_{-1}'(x)=1\ ,\\ &n_2'(x)=1+\tfrac{7}{3}[u_0+\gamma(x-x_0)]\ ,\\ &n_{-2}'(x)=1-\tfrac{7}{3}[u_0+\gamma(x-x_0)]\ ,\\ &n_3'(x)=2\{1+\tfrac{7}{3}[u_0+\gamma(x-1-x_0)]-\tfrac{7}{3}(\tau-1)\gamma\}\ ,\\ &n_{-3}'(x)=2\{1-\tfrac{7}{3}[u_0+\gamma(x+1-x_0)]-\tfrac{7}{3}(\tau-1)\gamma\}\ ,\\ &n_4'(x)=2\{1-\tfrac{7}{3}[u_0+\gamma(x-1-x_0)]+\tfrac{7}{3}(\tau-1)\gamma\}\ ,\\ &n_{-4}'(x)=2\{1+\tfrac{7}{3}[u_0+\gamma(x+1-x_0)]+\tfrac{7}{3}(\tau-1)\gamma\}\ , \end{aligned} \tag{24}$$

which are identical to the initial distribution [Eq. (23)]. Thus, these distributions are stationary.

At the boundary node ($x=0$), the incoming populations are

$$\begin{aligned} &n_0(0)=2,\quad n_1(0)=1,\quad n_{-1}(0)=1\ ,\\ &n_2(0)=1+\tfrac{7}{3}u_u,\quad n_{-2}(0)=1-\tfrac{7}{3}u_u\ ,\\ &n_3(0)=2(1+\tfrac{7}{3}u_u)\ ,\\ &n_{-3}(0)=2[1-\tfrac{7}{3}(u_0-\gamma x_0)-\tfrac{7}{3}\tau\gamma]\ ,\\ &n_4(0)=2(1-\tfrac{7}{3}u_u)\ ,\\ &n_{-4}(0)=2[1+\tfrac{7}{3}(u_0-\gamma x_0)+\tfrac{7}{3}\tau\gamma]\ . \end{aligned} \tag{25}$$

Using Eq. (3) and setting $u_u=u_0-\gamma x_0$, a choice that will be justified *a posteriori*, one obtains

$$\rho\mathbf{u}(0,t)=[56(u_0-\gamma x_0)+\tfrac{28}{3}\gamma\tau]\mathbf{e}_y\ . \tag{26}$$

Applying Eqs. (6), (7), and (20) with $\mathbf{u}_b=u_0\mathbf{e}_y$ and noting by t_{++} the time immediately after the LBE collisions *and* the momentum density exchange, we obtain the following distributions at the boundary:

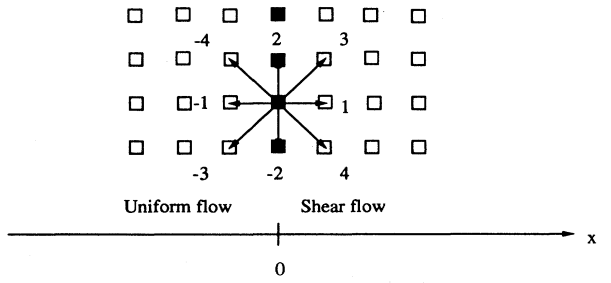

FIG. 6. Two-dimensional projection of the 14-link model and geometry of the problem considered. The open squares are the fluid nodes, the filled squares the boundary nodes of the wall. The weights of the velocity directions are $w_i=8$ for directions $i=\pm1,\pm2$ and the rest particle $i=0$, and $w_i=1$ for the diagonal directions $i=\pm3,\pm4$,

$$
\begin{aligned}
&n_0(0,t_{++})=2,\quad n_1(0,t_{++})=1,\quad n_{-1}(0,t_{++})=1\ ,\\
&n_2(0,t_{++})=1+\tfrac{7}{3}(u_0-\gamma x_0)+\tfrac{7}{3}\gamma(\tfrac{1}{6}-2x_0)\ ,\\
&n_{-2}(0,t_{++})=1-\tfrac{7}{3}(u_0-\gamma x_0)+\tfrac{7}{3}\gamma(\tfrac{1}{6}-2x_0)\ ,\\
&n_3(0,t_{++})=2\{1+\tfrac{7}{3}[u_0+\gamma(1-x_0)]-\tfrac{7}{3}\tau\gamma\}\\
&\qquad\qquad +2\tfrac{7}{3}\gamma(\tfrac{1}{6}-2x_0)\ ,\qquad (27)\\
&n_{-3}(0,t_{++})=2[1-\tfrac{7}{3}(u_0-\gamma x_0)]+2\tfrac{7}{3}\gamma(\tfrac{1}{6}-2x_0)\ ,\\
&n_4(0,t_{++})=2\{1-\tfrac{7}{3}[u_0+\gamma(1-x_0)]+\tfrac{7}{3}\tau\gamma\}\\
&\qquad\qquad +2\tfrac{7}{3}\gamma(\tfrac{1}{6}-2x_0)\ ,\\
&n_{-4}(0,t_{++})=2[1+\tfrac{7}{3}(u_0-\gamma x_0)]+2\tfrac{7}{3}\gamma(\tfrac{1}{6}-2x_0)\ .
\end{aligned}
$$

Propagating these distributions to the neighboring nodes, comparison with expressions (21) and (23) leads to the conclusion that the proposed distributions are stationary under the boundary rule if the width of the boundary layer is $x_0=\frac{1}{12}$. This result justifies the choice of $u_u=u_0-\gamma x_0$. We note that the width of the boundary layer is viscosity independent. By applying Eq. (3) to the above distributions, we obtain

$$\rho\mathbf{u}(0,t_{++})=[56(u_0-\gamma x_0)-\tfrac{28}{3}\gamma\tau+\tfrac{28}{3}\gamma]\mathbf{e}_y\ . \qquad (28)$$

The average velocity at the boundary node $\mathbf{u}_{\text{avg}}$ is

$$\mathbf{u}_{\text{avg}}=\frac{1}{\rho}\frac{\rho\mathbf{u}(0,t)+\rho\mathbf{u}(0,t_{++})}{2}=u_0\mathbf{e}_y \qquad (29)$$

($\rho=56$, $x_0=\frac{1}{12}$) and thus equal to the imposed node velocity u_0, as expected.

The force onto the wall resulting from the boundary rule is computed as

$$\mathbf{f}_{\text{wall}}=-[\rho\mathbf{u}(0,t_{++})-\rho\mathbf{u}(0,t_{+})]\ ; \qquad (30)$$

$\rho\mathbf{u}$ being a LBE collision invariant, we can substitute $\rho\mathbf{u}(0,t_+)$ with $\rho\mathbf{u}(0,t)$ and, using Eqs. (26) and (28), obtain ($\rho=56$)

$$\mathbf{f}_{\text{wall}}=[\tfrac{56}{6}(2\tau-1)\gamma]\mathbf{e}_y=\eta\gamma\mathbf{e}_y\ , \qquad (31)$$

where $\eta=\rho\nu$ is the viscosity of the fluid and the last identity derives from Eq. (8).

We have thus shown that by imposing a boundary velocity u_0 at the wall, a linear shear flow with velocity gradient γ is generated in the exterior field and the interior fluid (in the case of a solid particle simulation) moves at uniform velocity $u_0-\gamma/12$. A viscosity-independent boundary layer of width $\frac{1}{12}$ is set up. These results have been verified by numerical simulations of planar Couette flow [21]. The force per unit area onto the boundary is computed exactly for the linear shear flow considered here. It may be surprising that the uniform flow inside the particle does not have the expected velocity u_0 of the wall. However, the exact velocity distribution inside the particle is not physically relevant for the present simulations, whereas the exact computation of the forces on the particles is the essence of the procedure.

The analytical results presented here show the applicability of the method to a simple flow configuration. In order to test the method for particulate suspensions, we perform several numerical tests and compare our results to independent calculations [4].

The general methodology for these tests is discussed in detail in Ref. [6]. Before, however, presenting the results of these numerical simulations, we discuss the improvement we propose to the treatment of the so-called "shared boundary nodes." These nodes are boundary nodes shared between two adjacent particles, as illustrated in Fig. 3. The procedure for updating the distribution functions at the shared nodes described in Ref. [6] is to implement the usual momentum density exchange, using the average of the two local particle velocities as the boundary node velocity [Eq. (11)],

$$\mathbf{u}_b=\tfrac{1}{2}[\mathbf{U}_1+\Omega_1\times(\mathbf{r}_b-\mathbf{R}_1)+\mathbf{U}_2+\Omega_2\times(\mathbf{r}_b-\mathbf{R}_2)]\ . \qquad (32)$$

The resulting force is then divided equally between the two particles. As shown in Ref. [6], in the absence of shear stress inside the particles this procedure leads to zero force on the particles and has thus the same effect as allowing the distribution functions to pass freely from one particle to the other and not implementing the boundary rule at the shared nodes. A similar result is easily obtained for the present RBBN method. At steady state and in the absence of shear stress inside the particles, the local fluid velocity at the shared node is equal to the average of the local flow velocities inside the two particles and thus equal to $\mathbf{u}_b$ as constructed in Eq. (32). The force on the particles will, therefore, be zero. To simplify the procedure at the shared nodes, we thus suggest treating all shared boundary nodes as simple fluid nodes. As will be seen in the following, this simplification has proven successful.

The first test is the computation of the translational and rotational friction coefficients of a simple cubic lattice of spheres, obtained by imposing periodic boundary conditions on the unit cell containing a single sphere. As for the FM, the hydrodynamic radius of the particle is obtained from the translational drag at low volume fraction. The hydrodynamic radii are again averaged for about 100 different positions of the center of mass of the particle within the lattice to take into account the various possible configurations of boundary nodes, as discussed previously. The results are presented in Fig. 7, compared to independent numerical results that can be considered exact [4]. The agreement for the translational friction can be seen to be good over the whole range of volume fractions, even for very small particles with a radius of the order of three lattice spacings. The results for the rotational friction are clearly not as good at a high volume fraction, especially when compared with the results obtained by the BBL method in Ref. [6]. Large particles are needed to approach the expected result. The reason for this lies in the location of the boundary nodes. Generally, the resolution of the particles on the lattice is better with the BBL method than with the RBBN method; the discrete nature of the lattice is more markedly felt for the rotational friction because the surfaces of neighboring spheres (of the central sphere and its period-

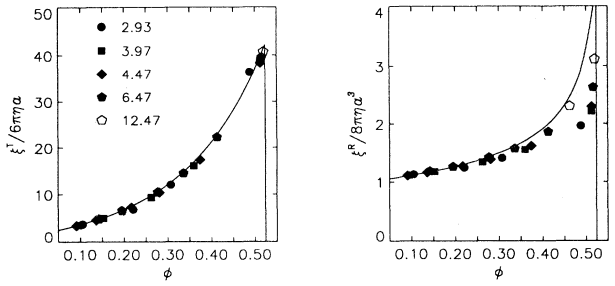

FIG. 7. Normalized translational (ξ^T) and rotational (ξ^R) friction coefficients for periodic arrays of spheres as a function of volume fraction. The coefficients have been normalized by the isolated-sphere result. The solid curves are results from independent numerical calculations [4]. The statistical errors are smaller than the plotting symbols.

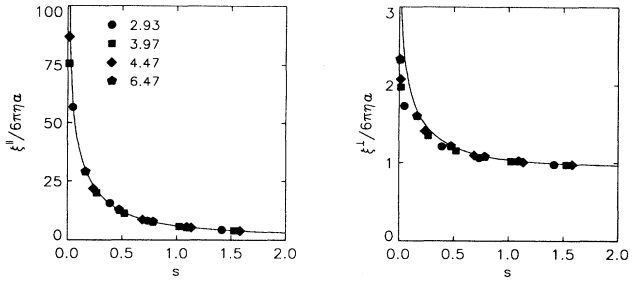

FIG. 8. Hydrodynamic interactions between pairs of spheres. The parallel ($\xi^{\parallel}$) and perpendicular ($\xi^{\perp}$) friction coefficients are plotted as function of the particle-particle distance $s=R_{12}/a_H-2$, where R_{12} is the center to center distance and a_H the hydrodynamic radius. The solid lines are independent numerical solutions [4]. The statistical errors are smaller than the plotting symbols.

ic images) are in relative motion and thus the exact shape of the surfaces is of importance. It was also seen in the above analysis of the boundary rule that the stick boundary condition does not exactly apply at the boundary node. The force densities $\mathbf{f}(\mathbf{r}_b)$ resulting from the momentum density exchange at the boundary are physically not applied at $\mathbf{r}_b$ but at the outer edge of the boundary layer $\mathbf{r}_b+x_0\mathbf{c}_i$. This has no influence on the total force applied onto the particle and the translational friction is thus obtained correctly. However, the total torque, obtained by summing $(\mathbf{r}_b-\mathbf{R})\times\mathbf{f}(\mathbf{r}_b)$ over the boundary nodes, will not reflect the true torque onto the particle. Again, this effect is diminished for large particles. However, as will be seen in what follows, this has no measurable consequences on the results obtained for the bulk transport properties of suspensions.

A more important test of the simulation method is the computation of the hydrodynamic forces between solid particles. We will consider here pairs of spheres in relative motion to each other. The lubrication forces, when the particles are close to contact, diverge as s^{-1} along the line of centers and as $\ln s^{-1}$ perpendicular to the line of centers, where $s=(R_{12}-2a)/a$ is the relative spacing between two particles of radius a and R_{12} the center-center distance. The two particles move with velocities $\mathbf{u}$ and $-\mathbf{u}$, respectively, either along their line of centers or perpendicular to it. Our results, presented in Fig. 8, are again averaged over particle positions (and thus sets of boundary nodes) and are compared to independent calculations of the hydrodynamic forces—including the lubrication forces—for an identical geometry [6]. The results obtained for the forces along the line of centers are in excellent agreement with those independent calculations. Even for interparticle separations of less than one lattice spacing, our results agree remarkably well with lubrication theory. This is a clear improvement over the results obtained in Ref. [6], where the required divergence of the lubrication forces was not reproduced for particle separations of less than one lattice spacing. However, it is not entirely clear if this improvement is due to the choice of boundary rules or to the treatment of the shared nodes, which will clearly be present at such small interparticle distances. The results for the transverse force are poorer, the reason for this being similar to the reasons affecting the rotational friction, mainly the rather poor resolution of the particles on the lattice obtained with the RBBN method. This has a bigger influence on surfaces that move parallel to each other than on surfaces moving towards each other.

As for the FM, we have computed three transport coefficients via dissipative methods: the inverse permeability of a fixed configuration (K^{-4}), the short-time collective mobility (μ), and the short-time self-diffusion (D_s). The normalized results are presented in Fig. 9. It is apparent that all three transport coefficients are ob-

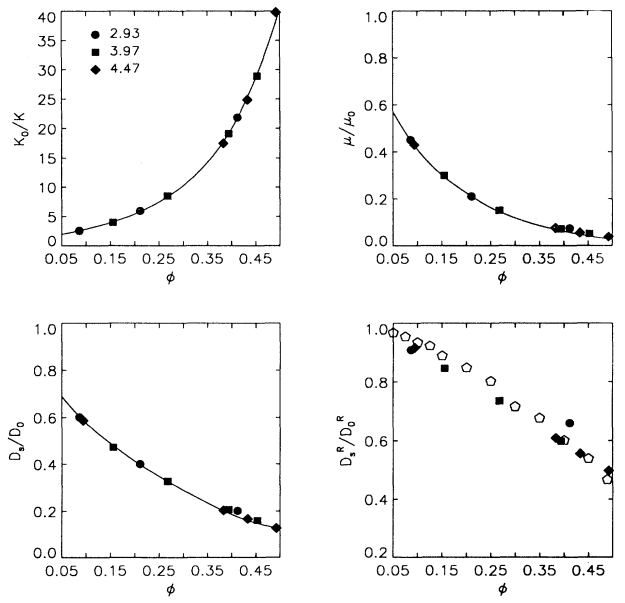

FIG. 9. Transport coefficients for 16 spheres as a function of volume fraction obtained with the RBBN method. Legend as in Fig. 5. The rotational self-diffusion D_s^R has been normalized by the isolated-sphere result D_0^R. The open symbols for the normalized rotational diffusion are the results from Ref. [23].

tained with very good accuracy over the whole concentration range and for particle radii not exceeding five lattice spacings. Thus, the limitations of the RBBN method noted above for the rotational drag and, to a lesser extent, for the two-body hydrodynamic interactions perpendicular to the line of centers do not seem to have any influence on the results of our computations of these transport coefficients. As a final test to see if the failure to correctly reproduce the rotational friction might have an influence on transport coefficients related to rotational movement, we have computed the short-time rotational diffusion coefficient for an equilibrium configuration of spheres. This was done by imposing an angular velocity Ω_1 on one particle in the configuration and measuring its steady-state torque T_1. The rotational mobility μ_R is

$$\mu_R = \frac{\Omega_1}{T_1} , \tag{33}$$

and the rotational self-diffusion is obtained from $D_s^R = k_B T \mu_R$, where k_B is the Boltzmann constant and T the temperature. We compare our results in Fig. 9 to those of Phillips, Brady, and Bossis [23], obtained via a Stokesian dynamics method that explicitly includes lubrication forces. The data is normalized by the isolated-sphere result $D_0^R = k_B T (8\pi\eta a_H^3)^{-1}$. As shown in Ref. [23], finite-size effects are negligible for this calculation and we compare our data for 16 spheres to their data for 27 spheres. To match the results of Ref. [23], quite large spheres are needed with our method. This was expected in view of our results for the rotational friction; however, the deviations from the results of Ref. [23] for a sphere with a radius of the order of 4.5 lattice spacings are never more than 10% and it appears that the difficulties encountered with rotational motion are less severe in random dispersions than in periodic lattice arrangements of spheres.

While the above results for the self-diffusion and the collective mobility have been obtained via a dissipative method, it is also possible to simulate "thermal" fluctuations in the fluid by adding random components to the fluid stress tensor [5,6]. The kinetic equation (1) is then modified to

$$n_i(\mathbf{r}+\mathbf{c}_i, t+1) = n_i(\mathbf{r},t) + \sum_j w_j \Delta_{ij} [n_j(\mathbf{r},t) - n_j^{\mathrm{eq}}(\mathbf{r},t)] + n_i'(\mathbf{r},t) , \tag{34}$$

where $n_i'(\mathbf{r},t)$ is chosen such that only its contribution to the fluid stress is nonzero,

$$n_i'(\mathbf{r},t) = C_i \sigma'_{\alpha\beta} \overline{c_{i\alpha}, c_{i\beta}} . \tag{35}$$

$\sigma'_{\alpha\beta}$ are the random stress fluctuations and are sampled from a Gaussian distribution whose variance fixes the temperature. C_i is a constant defined in Eq. (5). It is thus possible to simulate Brownian motion with the fluctuating lattice Boltzmann method and calculate the transport coefficients via Green-Kubo-type relations. If the fluctuation-dissipation theorem is obeyed, the results obtained via the fluctuating and the dissipative methods should agree with each other. The results presented in Ref. [6] suggest that fluctuation dissipation is not exactly obeyed at high solid concentrations with the BBL method—possibly due to the treatment of the shared nodes. We have done similar calculations with the RBBN method and the simplified treatment of the shared nodes described above. The short-time collective mobility (μ) and the short-time self-diffusion (D_s) are obtained from integrals over the velocity correlation functions of the particles [6]. In Table I, we compare the results for those two transport coefficients from the dissipative and the fluctuating method. As can be seen, fluctuation dissipation is obeyed at all volume fractions for particles with radii superior to about 3.5 lattice spacings and at low volume fraction for particles with radii as small as 2.5 lattice spacings. This is a clear improvement over the results reported in Ref. [6].

IV. CONCLUSIONS

We have studied different methods of treating the solid-liquid boundary in a lattice Boltzmann fluid in order to simulate solid-particle suspensions. It was seen that the generalized bounce-back rule as devised by Ladd [6] and Ladd and Frenkel [7,8] is only applicable when the boundary nodes are placed on the lattice links and

TABLE I. Comparison of results for the normalized short-time self-diffusion D_s/D_0 and the normalized collective mobility μ/μ_0 for 16 spheres between the dissipative and fluctuating methods. The radii are in lattice units and ϕ is the particle volume fraction.

		D_s/D_0		μ/μ_0	
Radius	ϕ	Dissipative	Fluctuating	Dissipative	Fluctuating
2.93	0.086	0.601±0.005	0.594±0.009	0.451±0.005	0.450±0.025
	0.211	0.400±0.005	0.404±0.009	0.210±0.003	0.235±0.035
	0.412	0.201±0.003	0.176±0.004	0.073±0.001	0.072±0.005
3.97	0.394	0.206±0.003	0.201±0.005	0.072±0.001	0.072±0.006
	0.453	0.159±0.003	0.153±0.006	0.051±0.001	0.050±0.001
4.47	0.383	0.203±0.003	0.202±0.005	0.075±0.001	0.074±0.001
	0.492	0.126±0.002	0.120±0.008	0.038±0.001	0.036±0.003

not on the lattice nodes. However, placing the boundary on the links [6] complicates the algorithm by requiring additional information to be passed in between lattice nodes. We have shown that the intuitively simple FM, in which the fluid distribution functions inside the solid particle are forced to their equilibrium value representing the local solid-body velocity, does not reproduce correctly the hydrodynamic forces between solid particles. We have then introduced a new boundary rule, the "relaxed bounce-back rule." This boundary method combines the generalized bounce-back rule at the lattice nodes with LBE collisions at *all* lattice nodes. The solid-fluid interactions are thus treated simply on the lattice nodes. Through numerical computation of friction coefficients, hydrodynamic forces and several transport coefficients of particle suspensions, it was shown that this new method constitutes a valid and worthwhile alternative to the bounce-back rule with boundary nodes on the links as pioneered by Ladd [6]. While the method proposed by Ladd is particularly successful in reproducing the rotational behavior of solid particles, the method proposed here, as well as being easier to implement, seems to perform better for translational motion. In addition, we have introduced a simplified treatment of the so-called "shared nodes" and a new definition of the set of boundary nodes associated with a given particle. Both changes simplify considerably the general LBE–solid-particle algorithm. When using a fluctuating LBE for the simulation of Brownian motion [5,6], those changes, together with our new boundary rule, allow for fluctuation dissipation to be obeyed exactly through the whole range of solid-particle volume fractions.

ACKNOWLEDGMENTS

Financial support by both the Swiss National Foundation for Scientific Research and Unilever Research, Port Sunlight, UK, is gratefully acknowledged. Most of this work was performed at the Lawrence Livermore National Laboratory, Livermore, CA and I would like to thank the ISCR for their hospitality. Also, I would like to thank Livermore Computing for the very generous amounts of computing time made available on their Meiko CS2 computer as well as P. B. Warren, P. N. Pusey, G. S. Pawley, and especially A. J. C. Ladd for very helpful discussions.

[1] J. Happel and H. Brenner, *Low-Reynolds Number Hydrodynamics* (Prentice-Hall, Inc., Englewood Cliffs, NJ, 1965).
[2] D. L. Ermack and J. A. McCammon, J. Chem. Phys. **69**, 1352 (1978).
[3] J. F. Brady and G. Bossis, Ann. Rev. Fluid. Mech. **20**, 111 (1988).
[4] A. J. C. Ladd, J. Chem. Phys. **88**, 5051 (1988); **90**, 1149 (1989); **93**, 3484 (1990).
[5] A. J. C. Ladd, Phys. Rev. Lett. **70**, 1339 (1993).
[6] A. J. C. Ladd, J. Fluid Mech. **271**, 285 (1994); 311 (1994).
[7] A. J. C. Ladd and D. Frenkel, in *Cellular Automata and Modeling of Complex Physical Systems,* edited by P. Manneville, N. Boccara, G. Y. Vichmac, and R. Bidaux, Springer Proceedings in Physics Vol. 46 (Springer, Berlin, 1990).
[8] A. J. C. Ladd and D. Frenkel, Phys. Fluids A **2**, 1921 (1990).
[9] R. Benzi, S. Succi, and M. Vergassola, Phys. Rep. **222**, 147 (1993).
[10] F. J. Higuera and J. Jimenez, Europhys. Lett. **9**, 663 (1989).
[11] U. Frisch, D. d'Humières, B. Hasslacher, P. Lallemand, Y. Pomeau, and J.-P. Rivet, Complex Systems **1**, 649 (1987).
[12] O. Behrend, R. Harris, and P. B. Warren, Phys. Rev. E **50**, 4586 (1994).
[13] S. Chapman and T. G. Cowling, *The Mathematical Theory of Non-Uniform Gases* (Cambridge University Press, Cambridge (1960).
[14] P. Bhatnager, E. P. Gross, and M. K. Krook, Phys. Rev. **94**, 511 (1954).
[15] Y. H. Qian, D. d'Humières, and P. Lallemand, Europhys. Lett. **17**, 479 (1992).
[16] S. Chen, Z. Wang, X. Shan, and G. D. Doolen, J. Stat. Phys. **68**, 379 (1992).
[17] R. Cornubert, D. d'Humières, and C. D. Levermore, Physica D **47**, 241 (1991).
[18] D. P. Ziegler, J. Stat. Phys. **71**, 1171 (1993).
[19] H. Hasimoto, J. Fluid. Mech. **5**, 317 (1959).
[20] S. Chen, M. Dembo, T. Lookman, and A. Lapedes (unpublished).
[21] P. B. Warren (private communication).
[22] C. W. J. Beenakker and P. Mazur, Physica A **120**, 388 (1983); **126**, 349 (1984).
[23] R. J. Phillips, J. F. Brady, and G. Bossis, Phys. Fluids **31**, 3462 (1988).